



Hydrothermal synthesis of $\text{In}_2\text{O}_3\text{-ZnO}$ nanocomposite and their enhanced photocatalytic properties

Wenkang Zhang¹ · Wenyi Huang¹ · Qixue Wu¹ · Hao Cheng^{1,2}

Received: 4 October 2021 / Accepted: 23 December 2021 / Published online: 29 January 2022
© The Author(s), under exclusive licence to Springer-Verlag GmbH, DE part of Springer Nature 2022

Abstract

In this study, an indium oxide–zinc oxide ($\text{In}_2\text{O}_3\text{-ZnO}$) nanocomposite is successfully synthesized via a facile hydrothermal process. The samples are characterized using X-ray diffraction, scanning electron microscopy, high-resolution transmission electron microscopy, ultraviolet–visible diffuse reflectance spectroscopy, Fourier–transform infrared spectroscopy, and so on. The photocatalytic test results show that the photocatalytic degradation of methyl orange efficiency of 15% $\text{In}_2\text{O}_3\text{-ZnO}$ nanocomposite can be more than 96.62% after 120 min, which is much higher than that of In_2O_3 and ZnO particles. The enhanced photocatalytic activity is attributed to the reduction in electrons (e^-) and holes (h^+) recombination in the photocatalytic process; it allows the rapid separation of photo-generated charge carriers, thus enhancing their photocatalytic activity. Finally, a possible photocatalytic reaction mechanism is proposed.

Keywords Hydrothermal synthesis · $\text{In}_2\text{O}_3\text{-ZnO}$ nanocomposite · Photocatalytic properties · Photocatalytic reaction mechanism

1 Introduction

Recently, the environmental pollution problem has become increasingly severe due to the rapid development of industries [1, 2]. A significant amount of industrial wastewater is discharged into the natural environment, and the sewage purification and treatment issues have attracted people's attention [2, 3]. Dyes have various applications and generates the most severe water pollution among diverse pollutants and are difficult to decompose [3]. Photocatalytic technology is considered one of the most promising approaches among various water pollution remediation methods [4, 5]. Relevant research results show that sunlight is a significant and sustainable strategy for degrading pollutants and producing highly efficient clean energy [6–8].

Oxide semiconductor photocatalysts, such as ZnO, In_2O_3 , and TiO_2 , have attracted much attention due to their potential applications in environmental protection and energy production [9–11]. ZnO, with a wide bandgap of 3.37 eV and electron binding energy (60 meV), is a promising solution in the field of environmental pollution, among other oxide semiconductor materials, and has certain applications in photocatalytic, conductive materials, chemical sensors, and gas sensors, particularly showing potential advantages in the photocatalytic degradation of dyes [12]. However, the recombination process of ZnO photogenerated carriers in the photocatalytic process is much faster than the transporting process, resulting in lower photocatalytic efficiency of ZnO [13, 14]. Researchers have investigated different strategies in the past few decades to improve the photocatalytic efficiency of ZnO, including doping, metal loading, and heterostructure construction [15–17]. Among them, the combination of two semiconductor types to form semiconductor composites is considered an effective and economical technology for degrading organic pollutants [18]. ZnO is combined with other semiconductor materials to form nanocomposites, and various interfacial interactions will produce new properties [19]. The formation of semiconductors with an appropriate band gap, band edges, and high lattice matching degrees in a nanocomposite can facilitate the separation

✉ Hao Cheng
iamchenghao@126.com

¹ Guangxi Key Laboratory of Green Processing of Sugar Resources, College of Biological and Chemical Engineering, Guangxi University of Science and Technology, Liuzhou 545006, China

² Province and Ministry Co-Sponsored Collaborative Innovation Center of Sugarcane and Sugar Industry, Nanning 530004, China

of photogenerated electrons and holes [20]. Zhao et al. [21] successfully synthesized ZnO nanocomposite doped with In_2O_3 using a microwave hydrothermal method, which beneficially reduced the electrons and holes recombination during the photocatalytic process and promoted the active substances ($\bullet\text{OH}$ and $\bullet\text{O}_2^-$). Martha et al. [22] successfully synthesized In_2O_3 -modified ZnO nanocomposite using a coprecipitation method, which demonstrated high photocatalytic activity. Liu et al. [23] successfully synthesized In_2O_3 -ZnO nanocomposite with heterostructure using a one-step hydrothermal method, which promoted the separation of photogenerated carriers. The construction of heterostructures in nanocomposites can significantly improve the performance of nanocomposites, however, the choice of semiconductor materials when constructing heterostructures is crucial.

In_2O_3 is an indirect band semiconductor with a 2.56 eV bandgap and is a highly effective sensitizer to extend the absorption spectra of the transition metal oxide photocatalyst from ultraviolet (UV) to the visible region [24, 25]. Its valence and conduction band arrangement is irregular compared with ZnO. Several studies have been reported on In_2O_3 -ZnO nanocomposites, which relate to organic compound degradation and photocatalysis hydrogen production [26, 27]. These results suggest that doping In_2O_3 into ZnO nanostructures can significantly inhibit the recombination of photogenerated electron-hole pairs to enhance photocatalysis. In addition, p-n junctions can also be formed at the interface between the ZnO and In_2O_3 phases in the In_2O_3 -ZnO nanocomposites, which help separate the electron and hole pairs [28]. Consequently, the fabrication of In_2O_3 -ZnO nanocomposites has attracted significant attention.

This study successfully synthesized In_2O_3 -ZnO nanocomposites with enhanced photocatalytic properties via a hydrothermal process. The microstructure, phase, and optical properties of the samples were investigated. The photocatalytic properties of the as-synthesized samples were investigated by the degradation of methyl orange (MO) in an aqueous solution under UV light irradiation. As anticipated, the obtained In_2O_3 -ZnO nanocomposite exhibits excellent charge separation efficiency and higher photocatalytic properties than In_2O_3 and ZnO particles. Concurrently, we proposed and discussed the charge transfer and probable photocatalytic mechanism.

2 Experimental details

2.1 Materials

All chemicals applied in this experiment including zinc nitrate hexahydrate ($\text{Zn}(\text{NO}_3)_2 \cdot 6\text{H}_2\text{O}$, Shandong West Asia

Chemical Industry Co., Ltd.), sodium hydroxide (NaOH), polyethylene glycol (PEG), indium nitrate, and ethanol were purchased and used without any further purification. All the chemical reagents are analytical grade. Highpurity deionized water was used throughout all experiments.

2.2 Preparation of ZnO nanoparticles

ZnO nanoparticles are synthesized using the hydrothermal process. First, $\text{Zn}(\text{NO}_3)_2 \cdot 6\text{H}_2\text{O}$ (5.950 g), NaOH (5.000 g), and PEG (2.000 g) are mixed and stirred for 1.5 h at room temperature to yield a white precipitate. Further, the precipitate is diverted into the Teflon autoclave and maintained for 6 h at 150 °C. The precipitate is then naturally cooled from 150 °C to room temperature, and the precipitate is washed three times using deionized water and ethanol anhydrous. Finally, the precipitate is vacuum-dried at 60 °C for 12 h, ground, and the dried samples are calcined at 500 °C for 2 h.

2.3 Preparation of In_2O_3 -ZnO nanocomposite

The experiment adopted the hydrothermal process to synthesize the In_2O_3 -ZnO nanocomposites. First, $\text{Zn}(\text{NO}_3)_2 \cdot 6\text{H}_2\text{O}$ (5.950 g), NaOH (5.000 g), and PEG (2.000 g) were mixed and stirred for 1.5 h at room temperature to yield a white precipitate. Further, $\text{Zn}(\text{NO}_3)_2 \cdot 6\text{H}_2\text{O}$ (5.950 g), NaOH (5.000 g), PEG (2.000 g), and indium nitrate (corresponding molar ratio: 0%, 1%, 2%, 5%, 10%, 15%, and 20%) are mixed and stirred for 1.5 h at room temperature, and the product is added to the above precipitate and stirred for 0.5 h at room temperature to yield a white precipitate. Afterward, the above precipitate is diverted into the Teflon autoclave and maintained for 6 h at 150 °C. In addition, the precipitate is naturally cooled from 150 °C to room temperature, and the precipitate is washed three times using deionized water and ethanol anhydrous. Finally, the precipitate is vacuum-dried at 60 °C for 12 h, ground, and the dried samples are calcined at 500 °C for 2 h.

2.4 Characterization

The crystal structures are studied using powder X-ray diffraction (XRD). The morphologies of the obtained samples are measured using scanning electron microscopy (SEM). The obtained samples are measured using high-resolution transmission electron microscopy (HRTEM) at an accelerating voltage of 200 kV. The ultraviolet-visible diffused reflectance spectra (UV-Vis DRS) of the samples are obtained using a spectrophotometer.

2.5 Photocatalytic properties test

The photocatalytic activities of the as-synthesized samples are evaluated by the photocatalytic degradation of MO. First, 50 mg of the photocatalysts is ultrasonically dispersed in 50 mL of 10 mg L⁻¹ MO aqueous solution. It is magnetically stirred in the dark for 30 min. Further, UV light irradiation is conducted using a 420-W Mercury lamp as the light source. At specified intervals, 4 mL aliquots are analyzed by obtaining variations in the absorption band (464 nm) in the UV-Vis spectra of MO.

3 Results and discussion

3.1 Structural and morphological characterization

Figure 1 shows the XRD patterns of pure ZnO and In₂O₃-ZnO nanocomposites. The diffraction peaks of pure ZnO at 31.79°, 34.44°, 36.27°, 47.56°, 56.63°, 62.87°, 66.40°, 67.92°, and 68.99° in 2θ correspond to the ZnO hexagonal wurtzite structure (100), (002), (101), (102), (110), (103), (200), (112), and (201) crystal planes, respectively, which are consistent with PDF (JCPDS NO. 36-1451) [29]. All diffraction peaks in the pure ZnO pattern can be expressed as a hexagonal phase structure [29]. The diffraction profile of In₂O₃-ZnO nanocomposites shows that the nanocomposites are composed of the hexagonal phase of ZnO (JPCDS, 36-1451) and the body-centered cubic structure of In₂O₃ (JCPDS, 71-2194). The 15% In₂O₃-ZnO spectrum line in the figure shows that the diffraction peak at

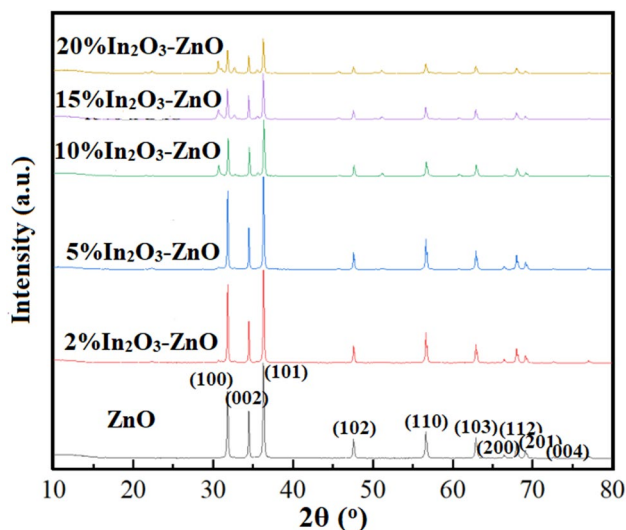


Fig. 1 XRD patterns of pure ZnO and In₂O₃-ZnO nanocomposites
2θ of 30.68°, 32.71°, 35.51°, 45.77°, 51.13°, and 60.84°

is consistent with that of PDF (JCPDS NO. 06-0415), except for the characteristic peak of ZnO, which may be In₂O₃ diffraction peaks, indicating that the In₂O₃-ZnO nanocomposite is an In₂O₃ cubic ferromanganese structure (C-In₂O₃) [30]. The diffraction peak intensity and crystallinity of C-In₂O₃ gradually increase with the C-In₂O₃ content, whereas the diffraction peak intensities of ZnO gradually decrease, which may imply that the characteristic peaks of ZnO are inhibited by the In₂O₃ composite ZnO. The sharp and intense diffraction peaks show that the samples are highly crystalline [31].

Figure 2 shows the SEM images (a and b) and particle size (c and d) of pure ZnO (a, c) and 15% In₂O₃-ZnO nanocomposite (b, d). Figure 2a shows that the pure ZnO are spindle particles, with a 200-nm-length and 100-nm-diameter. Figure 2b shows that the spherical small particles in the 15% In₂O₃-ZnO nanocomposite adhere to the spindle-like ZnO crystal. These small particles are In₂O₃ nanoparticles with a particle size of about 30 nm. The morphology and size of the spindle-like ZnO particles remain unchanged. This may be because the ZnO crystal size is not affected by the In₂O₃ composite, and the In₂O₃ nanoparticles adhere to the ZnO surface and form a composite with it [32]. Figure 2c and d shows that the particle size distributions of pure ZnO and 15% In₂O₃-ZnO nanocomposite are obviously narrowed, and the particles are more uniform.

Figure 3 shows the EDS diagram of the 15% In₂O₃-ZnO nanocomposite. The mass of Zn, In, and O elements present in the In₂O₃-ZnO nanocomposite are about 67.91%, 17.05%, and 15.04%, respectively, which is consistent with the theoretical mass percentage of 15% In₂O₃-ZnO nanocomposite, indicating that In₂O₃ and ZnO are aggregated as composite [33].

Figure 4 shows the TEM (a) and (c) and HRTEM (b) and (d) images of pure ZnO (a, b) and 15% In₂O₃-ZnO nanocomposite (c, d). Figure 4a and c show that ZnO and 15% In₂O₃-ZnO nanocomposite are composed of nanoparticles with a particle diameter of 25~30 nm. The HRTEM image of ZnO and 15% In₂O₃-ZnO is shown in Fig. 4b and d, and the clear lattice stripes can be observed, which indicates the high crystallinity of hexagonal ZnO and the high crystallinity of cubic In₂O₃ and hexagonal ZnO.

3.2 UV-Vis DRS analysis

Figure 5 shows the UV-Vis DRS of ZnO and 15% In₂O₃-ZnO nanocomposite. The 15% In₂O₃-ZnO nanocomposite absorption in the UV region is considerably more than ZnO and may improve the ZnO's absorption capacity in the UV region. Further, a redshift occurs along the 15% In₂O₃-ZnO nanocomposite absorption band, probably due to the increase in the visible light absorption range of the In₂O₃ composite ZnO [34].

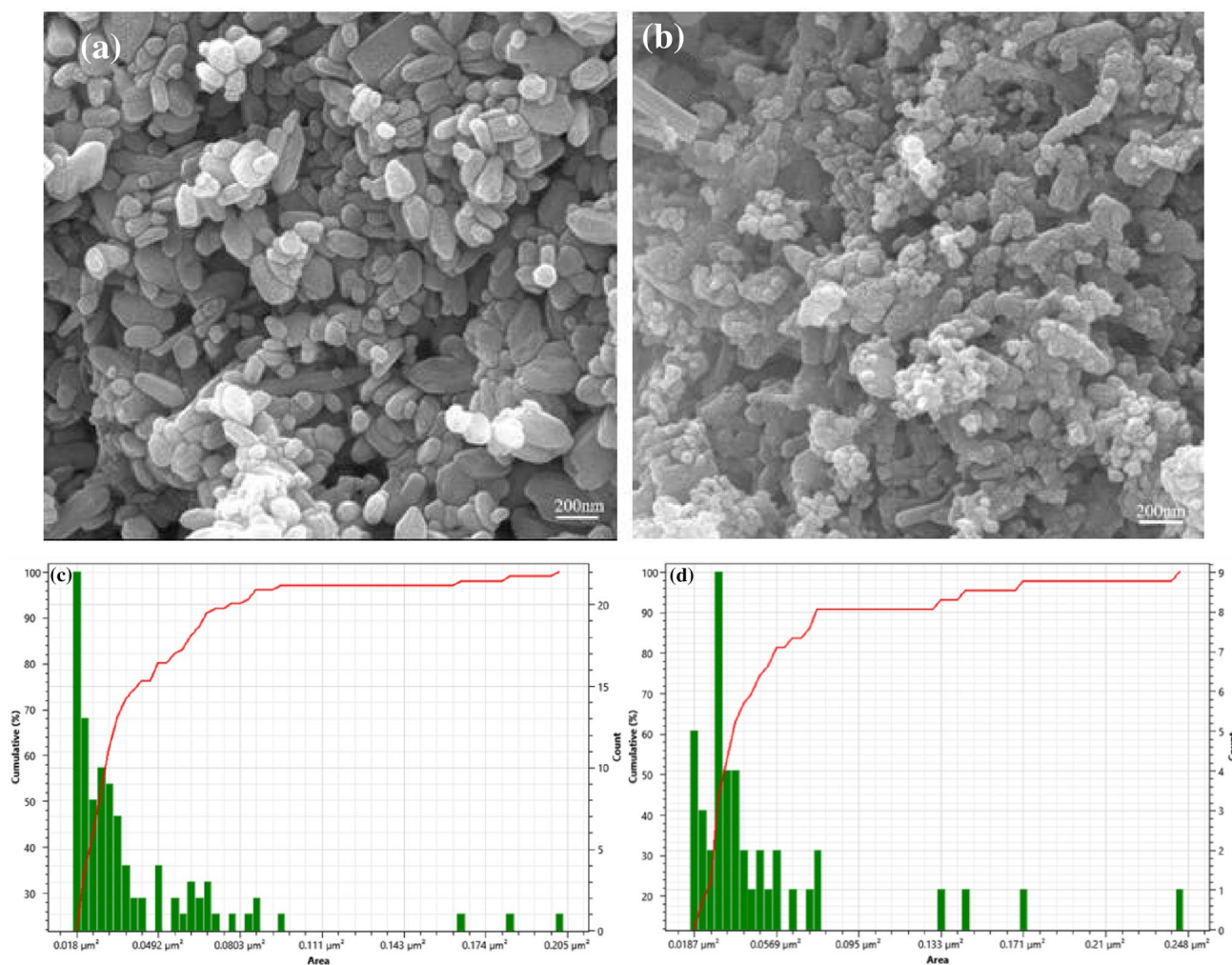


Fig. 2 SEM images **a** and **b** and particle size **c** and **d** of pure ZnO (**a, c**) and 15% In_2O_3 -ZnO nanocomposite (**b, d**)

3.3 FTIR analysis

Figure 6 shows the FTIR results of ZnO and 15% In_2O_3 -ZnO nanocomposite. The characteristic peaks of ZnO and 15% In_2O_3 -ZnO nanocomposite at 506 correspond to Zn-O peak [35]. The characteristic peaks of the 15% In_2O_3 -ZnO nanocomposite at 600 and 1158 cm^{-1} correspond to the In_2O_3 characteristic and $\delta(\text{OH})$ vibration peaks [36], respectively. The characteristic peaks of ZnO and 15% In_2O_3 -ZnO nanocomposite at 866 correspond to $\nu(\text{OH})$ vibration peak [35]. The ZnO characteristic peaks at 840 and 902 cm^{-1} correspond to the $\nu(\text{OH})$ and $\delta(\text{OH})$ vibration peaks, respectively [36]. The characteristic peaks of ZnO and 15% In_2O_3 -ZnO nanocomposite at 1385 cm^{-1} correspond to $\text{Zn}(\text{OH})_2$ vibration peak [35]. The characteristic peaks of ZnO and 15% In_2O_3 -ZnO nanocomposite at 1454 and 1439 cm^{-1} , respectively, correspond to the O-H bond bending vibration peaks, resulting in the absorption of atmospheric moisture from

the sample [35]. The wide characteristic peaks of ZnO and 15% In_2O_3 -ZnO nanocomposite at 3503 and 3515 cm^{-1} , respectively, may correspond to vibration peaks of product crystalline water or hydroxy hydroxide bending [36].

3.4 Photocatalytic activity and stability

Photocatalytic activity of In_2O_3 -ZnO nanocomposites is evaluated by MO degradation under UV light. Figure 7 shows the experimental results of the MO photocatalytic degradation in ZnO and In_2O_3 -ZnO nanocomposites. The degradation of MO in In_2O_3 , ZnO, and In_2O_3 -ZnO nanocomposites is very slow in the first 20 min. This shows that the adsorption capacity of In_2O_3 , ZnO, and In_2O_3 -ZnO nanocomposites to MO is relatively weak. The MO photocatalyst degradation rate in ZnO and In_2O_3 after 120 min are 83.31% and 81.56%, respectively, which are attributed to its high bandgap energy, indicating that ZnO and In_2O_3 have

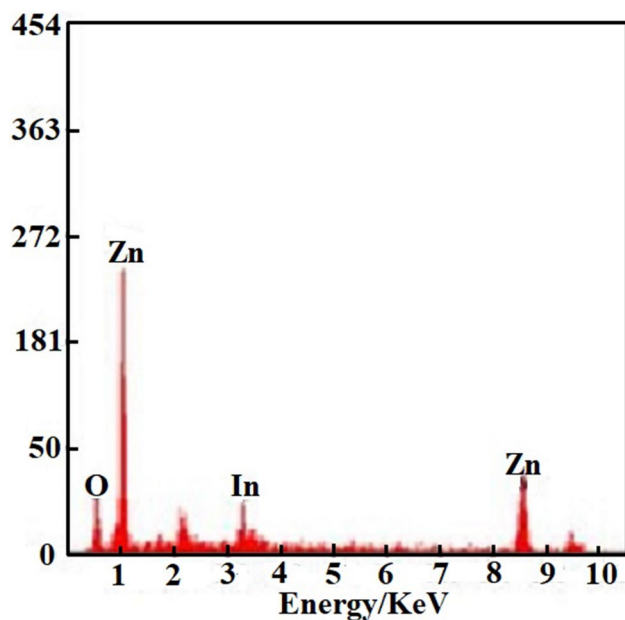


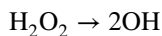
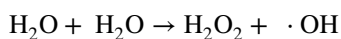
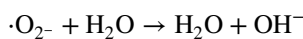
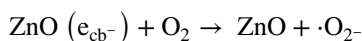
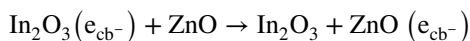
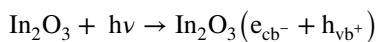
Fig. 3 EDS diagram of the 15% In₂O₃-ZnO nanocomposite

certain photocatalytic activities in the UV region. Alternatively, the MO degradation rate in In₂O₃-ZnO nanocomposites first increases after 120 min before decreasing with the percentage content; In₂O₃ composite ZnO may promote the transfer of photoelectron, inhibit the recombination of photoelectron-hole pairs, and improve the photocatalytic activity, indicating that an optimal percentage content is essential for enhancing the photocatalytic activity of In₂O₃-ZnO nanocomposites [37]. In₂O₃ and ZnO promote the recombination of photogenerated electron-hole pairs when the percentage content reaches a certain level, thereby reducing their photocatalytic activity. The photocatalytic activity of 15% In₂O₃-ZnO nanocomposite is the highest among others, and the MO degradation rate under UV light after 120 min was up to 96.62%. The results show that the appropriate content of nanocomposites allows for rapid separation of photogenerated charge carriers, thus enhancing their photocatalytic activity.

ZnO has poor stability in degrading organic pollutants. Therefore, investigating the photostability and repeatability of ZnO-based photocatalyst is critical. The recycling experiment is conducted using 15% In₂O₃-ZnO nanocomposite degradation of MO solution under UV irradiation [38]. Figure 8 shows the degradation efficiency of MO decreased from 96.62 to 92.02% after three cycles. Therefore, 15% In₂O₃-ZnO nanocomposite is stable in the photodegradation of organic pollutants.

3.5 Proposed photocatalytic mechanism

A mechanism is proposed to explain the enhanced photocatalytic performance of In₂O₃-ZnO nanocomposite based on the aforementioned results [39]. The photocatalytic performance of In₂O₃-ZnO nanocomposite is stronger than that of pure In₂O₃ and pure ZnO. This is primarily because under ultraviolet radiation, the In₂O₃ nanoparticles can absorb ultraviolet light and excite their own electrons, while ZnO conduction band is located between In₂O₃ conduction and valence bands. Thereupon, the photoexcited electrons on the surface of In₂O₃ can be easily transferred to the conduction band of ZnO, and the photoexcited holes remain on In₂O₃. In this way, photogenerated electrons and holes can be effectively separated, further improving their photocatalytic performance. In addition, due to the excellent crystallization performance of In₂O₃, electron migration has limited resistance, which is conducive to the effective separation of photogenerated electron-hole pairs, so as to increase the lifetime of loaded streamer. The bottom and top of the conduction band (CB) and valence band (VB) of ZnO are at -0.4 and 2.8 eV, respectively, whereas the bottom and top of the CB and VB of In₂O₃ are at -0.63 and 2.17 eV, respectively. Figure 9 shows that the bottom and top of the CB and VB of ZnO are located below those of In₂O₃. Further, In₂O₃ can be excited by UV light when combined with ZnO, and electrons in In₂O₃ migrate to the ZnO CB. In addition, the electron transport resistance is extremely low, and electron-hole recombination is reduced due to the high crystallinity of In₂O₃. Therefore, effective charge separation increases the lifetime of charge carriers and improves the efficiency of interfacial charge transfer to the adsorption matrix, resulting in higher photocatalytic activity of In₂O₃-ZnO nanocomposite. The suitable substrate can be oxidized and the original In₂O₃ recycled since the In₂O₃ (h⁺) radical redox potential is about 2.17 eV. In our experiment, the MO photocatalytic degradation mechanism is proposed as follows:



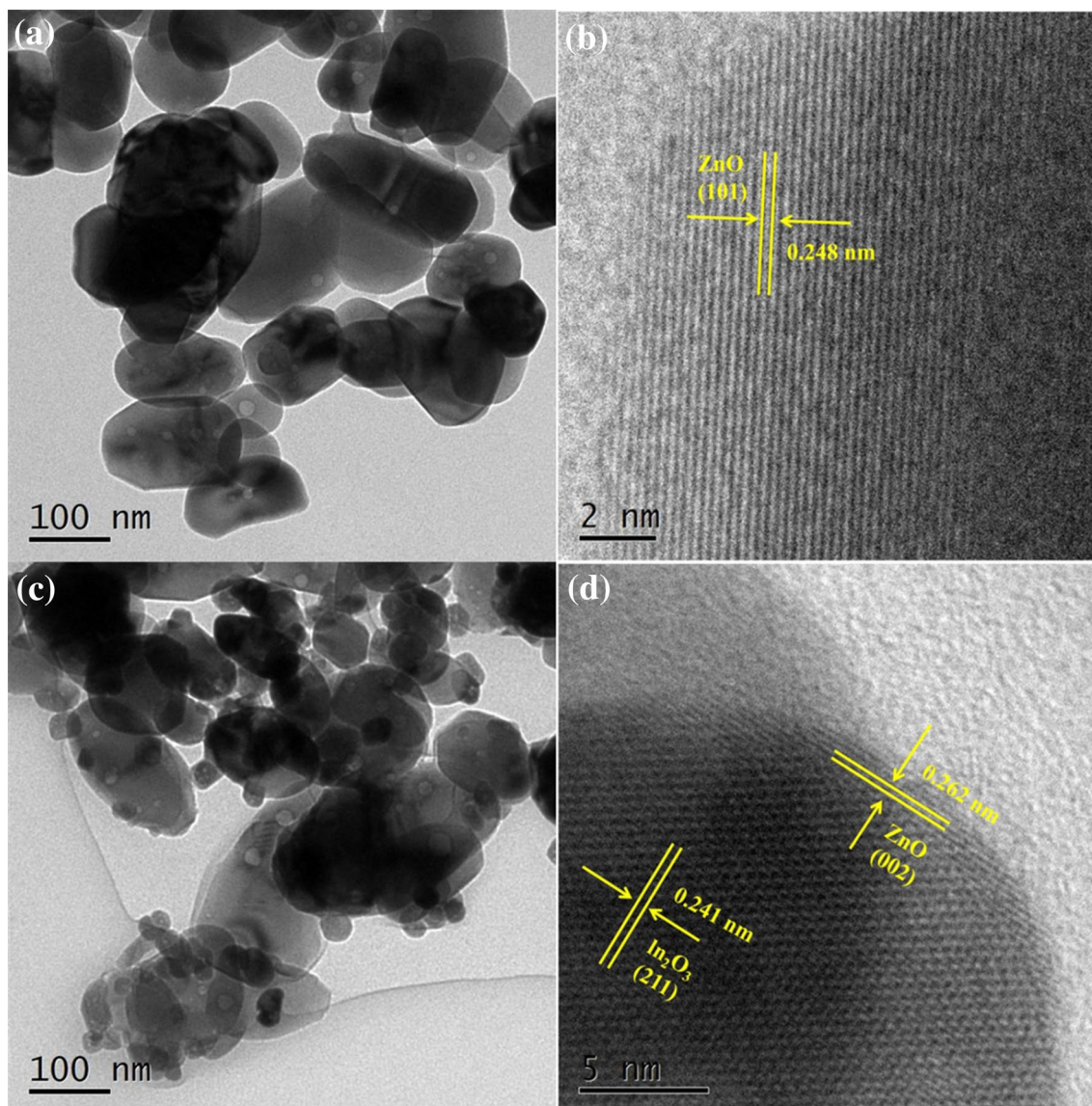


Fig. 4 TEM (a, c) and HRTEM (b, d) images of pure ZnO (a, b) and 15% In_2O_3 -ZnO nanocomposite (c, d)

$\cdot\text{OH} + \text{MO} \rightarrow \text{Degradation products}$

Under UV light, the photogenerated electrons in In_2O_3 move freely to the ZnO, whereas the photogenerated holes remain in the In_2O_3 VB. Dissolved oxygen molecules react with ZnO surface electrons to generate superoxy radical anion $\cdot\text{O}_2^-$, which produces hydrogen peroxide radical $\text{HO}_2\cdot$ at protonation, thus producing hydroxyl $\text{OH}\cdot$, which is a strong oxidizer that decomposes organic dyes [40].

4 Conclusions

The In_2O_3 -ZnO nanocomposite is successfully synthesized using the hydrothermal method. XRD analysis reveals that the In_2O_3 composite ZnO suppressed the ZnO characteristic peaks. SEM analysis shows that spindle-like ZnO crystal size in In_2O_3 -ZnO nanocomposite did not change due to In_2O_3 composite. EDS analysis reveals that the Zn, In, and O in the In_2O_3 -ZnO nanocomposite has a percent mass fraction of 15%. TEM analysis shows that 15% In_2O_3 -ZnO

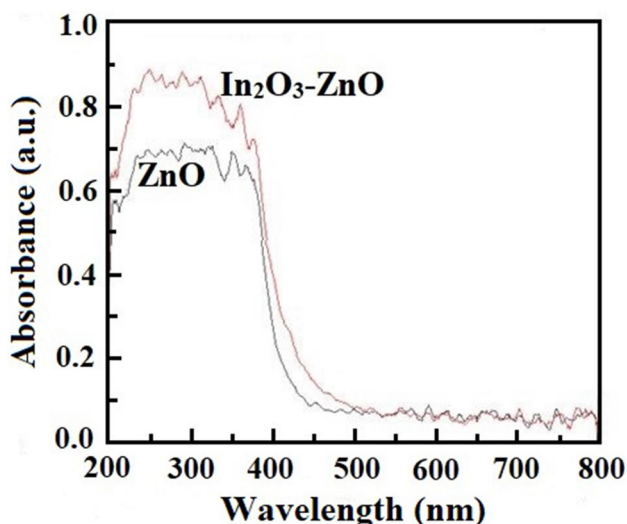


Fig. 5 UV-Vis DRS of ZnO and 15% $\text{In}_2\text{O}_3\text{-ZnO}$ nanocomposite

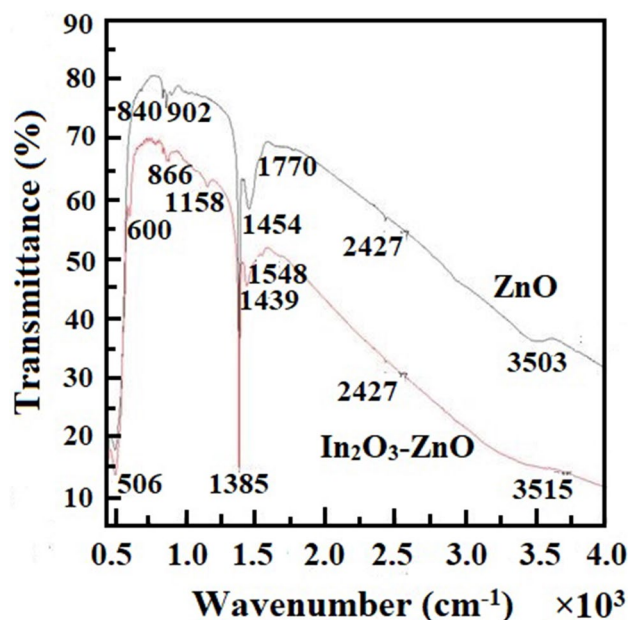
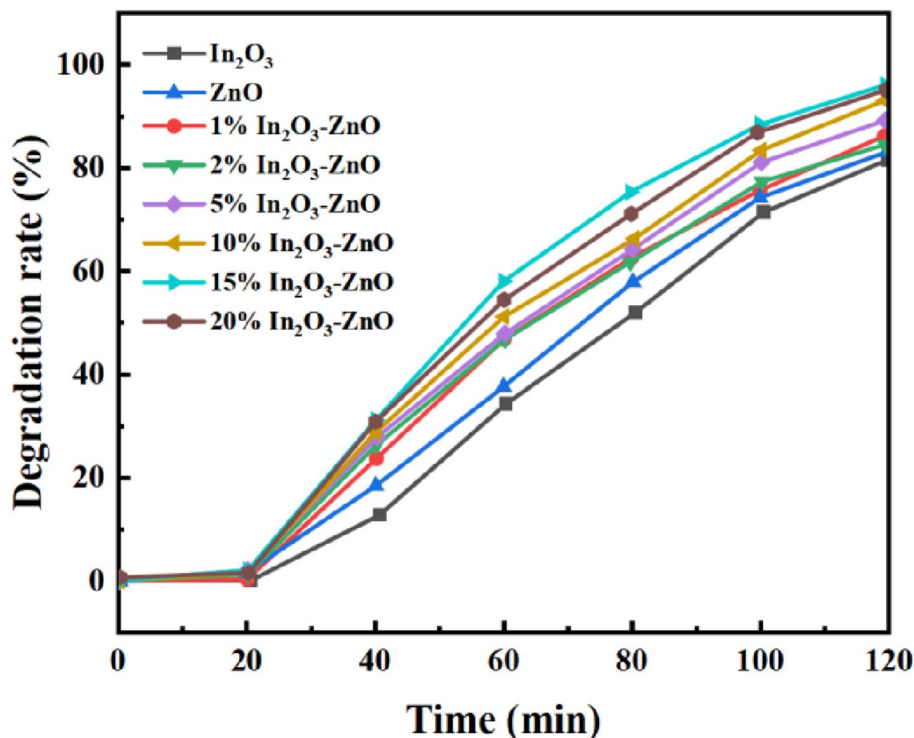


Fig. 6 FTIR results of ZnO and 15% $\text{In}_2\text{O}_3\text{-ZnO}$ nanocomposite

nanocomposite is composed of nanoparticles with a particle diameter of 25~30 nm. UV-Vis DRS analysis shows that In_2O_3 composite ZnO can broaden the range of ZnO visible light absorption. FTIR analysis reveals that the ZnO and In_2O_3 phases in $\text{In}_2\text{O}_3\text{-ZnO}$ nanocomposites exist individually. The experimental results of photocatalytic degradation

show that the photocatalytic activity of 15% $\text{In}_2\text{O}_3\text{-ZnO}$ nanocomposite is the best, and the MO degradation rate after 120 min can be up to 96.62%, thereby improving ZnO's photocatalytic performance.

Fig. 7 Experimental results of the MO photocatalytic degradation in ZnO and $\text{In}_2\text{O}_3\text{-ZnO}$ nanocomposites



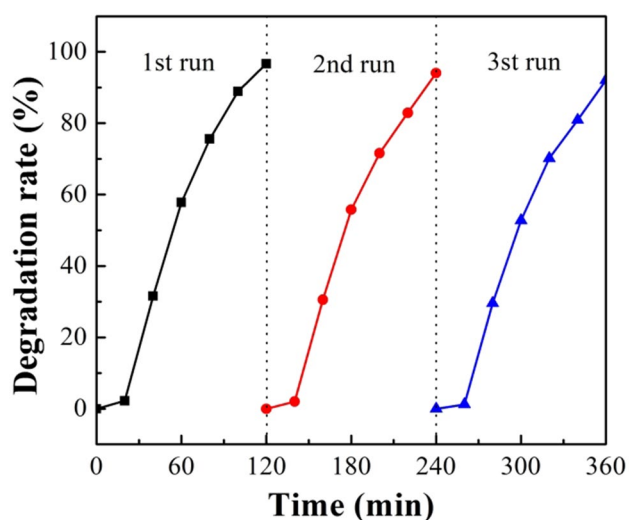


Fig. 8 Degradation efficiency of 15% In_2O_3 -ZnO nanocomposite for MO after three cycles

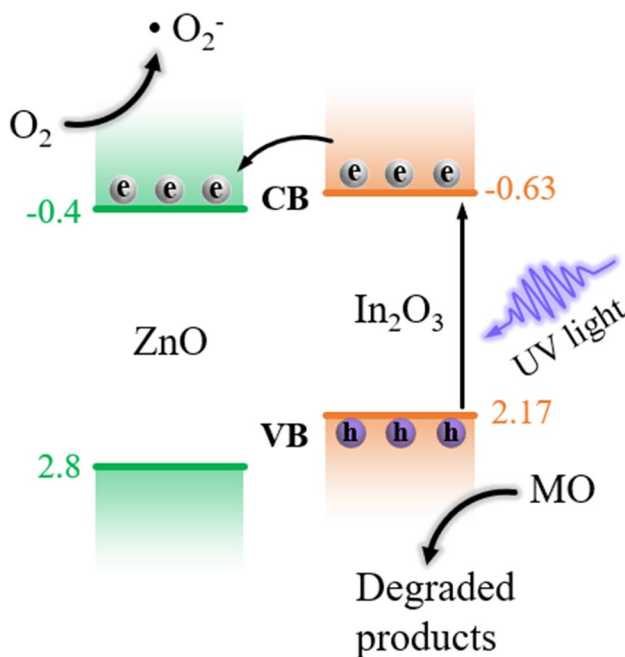


Fig. 9 Photocatalytic mechanism scheme of In_2O_3 -ZnO nanocomposite

Acknowledgements The authors gratefully acknowledge financial support from the National Natural Science Foundation of China (No. 21968005), the Opening Project of Guangxi Key Laboratory of Green Processing of Sugar Resources (No. GXTZY201701), and the High Levels of Innovation Team and Excellence Scholars Program in Colleges of Guangxi (Gui Jiaoren [2014] No. 7).

Data availability All data used to support this study are included within the paper.

Declarations

Conflict of interest The authors declare no conflicts of interest.

References

1. M. Lan, G. Fan, L. Yang, F. Li, Enhanced visible-light-induced photocatalytic performance of a novel ternary semiconductor coupling system based on hybrid Zn-In mixed metal oxide/g- C_3N_4 composites. *RSC Adv.* **5**, 5725 (2015)
2. C.B. Ong, L.Y. Ng, A.W. Mohammad, A review of ZnO nanoparticles as solar photocatalysts: synthesis, mechanisms and applications. *Renew. Sustain. Energy Rev.* **81**, 536–551 (2018)
3. W. K. Zhang, Q. Y. Zhong, X. M. Liu, Q. Lu, Inorganic functionalization of $\text{CdSe}_x\text{S}_{1-x}/\text{ZnS}$ core-shell quantum dots and their photoelectric properties. *Physica Status Solidi (A)*. **217**, 2000010 (2020)
4. H. Cheng, W.K. Zhang, X.M. Liu, T.F. Tang, J.H. Xiong, Fabrication of titanium dioxide/carbon fiber (TiO_2/CF) composites for removal of methylene blue (MB) from aqueous solution with enhanced photocatalytic activity. *J. Chem.* **9**, 1–11 (2021)
5. H. Cheng, X.N. Li, T.H. Li, D.F. Qin, T.F. Tang, Y.Q. Li, G.X. Wang, Electrospun nanofibers with high specific surface area to prepare modified electrodes for electrochemiluminescence detection of azithromycin. *J. Nanomater.* **93**, 1–10 (2021)
6. X.M. Liu, F.I. Chowdhury, L. Meng, Q. Xu, X. Wang, Luminescent films employing quantum dot-cellulose nanocrystal hybrid nanomaterials. *Mater. Lett.* **294**, 129737 (2021)
7. X.M. Liu, Q.Y. Zhong, W.M. Guo, W.K. Zhang, Y.Y. Ya, Y.Q. Xia, Novel platycladus orientalis-shaped Fe-doped ZnO hierarchical nanoflower decorated with Ag nanoparticles for photocatalytic application. *J. Alloys Compd.* **880**, 160501 (2021)
8. X.M. Liu, Y. Liu, W.K. Zhang, Q.Y. Zhong, X.Y. Ma, In situ self-assembly of 3D hierarchical 2D/2D $\text{CdS}/\text{g-C}_3\text{N}_4$ heterojunction with excellent photocatalytic performance. *Mater. Sci. Semicond. Process.* **105**, 104734 (2020)
9. X. M. Liu, S. B. Yao, Y. Liu, W. K. Zhang, F. M. Fu, H. Y. He, Metal ion-induced synthesis of hierarchical ZnO architectures with various morphologies and their photocatalytic performances. Springer Singapore. (2017).
10. H.R. Liu, C.J. Hu, H.F. Zhai, J. Yang, X.G. Liu, H.S. Jia, Fabrication of $\text{In}_2\text{O}_3/\text{ZnO}@\text{Ag}$ nanowire ternary composites with enhanced visible light photocatalytic activity. *RSC Adv.* **7**, 37220–37229 (2017)
11. N. Talebian, M.R. Nilforoushan, Z. Salehi, Effect of heterojunction on photocatalytic properties of multilayered ZnO-based thin films. *Ceram. Int.* **38**, 4623–4630 (2012)
12. S.G. Kumar, K.S.R.K. Rao, Comparison of modification strategies towards enhanced charge carrier separation and photocatalytic degradation activity of metal oxide semiconductors (TiO_2 , WO_3 and ZnO). *Appl. Surf. Sci.* **391**, 124–148 (2017)
13. X. Xiang, L.S. Xie, Z.W. Li, F. Li, Ternary $\text{MgO}/\text{ZnO}/\text{In}_2\text{O}_3$ heterostructured photocatalysts derived from a layered precursor and visible-light-induced photocatalytic activity. *Chem. Eng. J.* **221**, 222–229 (2013)
14. N. Talebian, M.R. Nilforoushan, R.R. Ghasem, Enhanced photocatalytic activities of ZnO thin films: a comparative study of hybrid semiconductor nanomaterials. *J. Sol-Gel. Sci. Technol.* **64**, 36–46 (2012)
15. N. Talebian, M.R. Nilforoushan, Comparative study of the structural, optical and photocatalytic properties of semiconductor metal oxides toward degradation of methylene blue. *Thin Solid Films* **518**, 2210–2215 (2010)

16. X.N. Liu, Q.F. Lu, J.H. Liu, Electrospinning preparation of one-dimensional ZnO/Bi₂WO₆ heterostructured sub-microbelts with excellent photocatalytic performance. *J. Alloys Compd.* **662**, 598 (2016)
17. C. Han, M.Q. Yang, B. Weng, Y.J. Xu, Improving the photocatalytic activity and anti-photocorrosion of semiconductor ZnO by coupling with versatile carbon. *Phys. Chem. Chem. Phys.* **16**, 16891 (2014)
18. Y.L. Xing, W.X. Que, X.T. Yin, Z.L. He, X.B. Liu, Y.W. Yang, J.Y. Shao, L.B. Kong, In₂O₃/Bi₂Sn₂O₇ heterostructured nanoparticles with enhanced photocatalytic activity. *Appl. Surf. Sci.* **387**, 36–44 (2016)
19. F. Zhao, Q. F. Lu, Z. L. Xiu, C. F. Zhu, Preparation and photocatalytic performance of one-dimensional In₂O₃ nanofibers, CuO microfibers and CuO/In₂O₃ heterostructured nanofibers by electrospinning process. *Nano: brief reports and reviews*, 11, 1650048 (2016)
20. M.M. Sun, Z.Y. Chen, Enhanced photoelectrochemical cathodic protection performance of the In₂O₃/TiO₂ composite. *J. Electrochem. Soc.* **162**, C96–C104 (2015)
21. J.K. Zhao, S.S. Ge, D. Pan, Y.L. Pan, V. Murugadoss, R. Li, W. Xie, Y. Lu, T.T. Wu, E.K. Wujcik, Q. Shao, X.M. Mai, Z.H. Guo, Microwave hydrothermal synthesis of In₂O₃-ZnO nanocomposites and their enhanced photoelectrochemical properties. *J. Electrochem. Soc.* **166**, H3074–H3083 (2019)
22. S. Martha, K.H. Reddy, K.M. Parida, Fabrication of In₂O₃ modified ZnO for enhancing stability, optical behaviour, electronic properties and photocatalytic activity for hydrogen production under visible light. *J. Mater. Chem. A* **2**, 3621–3631 (2014)
23. H.R. Liu, X. He, Y.C. Hu, X.G. Liu, H.S. Jia, B.S. Xu, One-step hydrothermal synthesis of In₂O₃-ZnO heterostructural composites and their enhanced visible-light photocatalytic activity. *Mater. Lett.* **131**, 104–107 (2014)
24. N. Lu, C.L. Shao, X.H. Li, F.J. Miao, K.X. Wang, Y.C. Liu, A facile fabrication of nitrogen-doped electrospun In₂O₃ nanofibers with improved visible-light photocatalytic activity. *Appl. Surf. Sci.* **391**, 668–676 (2017)
25. F. Zhao, Q.F. Lu, S.W. Liu, Preparation and characterization of In₂O₃/ZnO heterostructured microbelts by sol-gel combined with electrospinning method. *J. Sol-Gel. Sci. Technol.* **69**, 357–363 (2014)
26. F.L. Zhou, X.J. Li, J. Shu, J. Wang, Synthesis and visible light photo-electrochemical behaviors of In₂O₃-sensitized ZnO nanowire array film. *J. Photochem. Photobiol., A* **219**, 132–138 (2011)
27. Z.Y. Wang, B.B. Huang, Y. Dai, X.Y. Qin, X.Y. Zhang, P. Wang, H.X. Liu, J.X. Yu, Highly photocatalytic ZnO/In₂O₃ heteronanostructures synthesized by a coprecipitation method. *The Journal of Physical Chemistry C* **113**, 4612–4617 (2009)
28. F. Zhao, Q.F. Lu, S.W. Liu, C.Q. Wang, In₂O₃/ZnO heterostructured nanotubes: electrospinning fabrication, characterization, and highly enhanced photocatalytic properties. *J. Sol-Gel. Sci. Technol.* **72**, 137–143 (2014)
29. B.X. Li, T.X. Liu, Y.F. Wang, Z.F. Wang, ZnO/graphene-oxide nanocomposite with remarkably enhanced visible-light-driven photocatalytic performance. *J. Colloid Interface Sci.* **377**, 114–121 (2012)
30. Y.X. Du, P. Ding, Synthesis and cathodoluminescence of In₂O₃-SnO₂ nanowires heterostructures. *J. Alloy. Compd.* **507**, 456–459 (2010)
31. Q.P. Luo, X.Y. Yu, B.X. Lei, H.Y. Chen, D.B. Kuang, C.Y. Su, Reduced graphene oxide-hierarchical ZnO hollow sphere composites with enhanced photocurrent and photocatalytic activity. *J. Phys. Chem. C* **116**, 8111–8117 (2012)
32. J.B. Mu, C.L. Shao, Z.C. Guo, Z.Y. Zhang, M.Y. Zhang, P. Zhang, B. Chen, Y.C. Liu, High Photocatalytic activity of ZnO-carbon nanofiber heteroarchitectures. *ACS Appl. Mater. Interfaces* **3**, 590–596 (2011)
33. S. Rehman, R. Ullah, A.M. Butt, N.D. Gohar, Strategies of making TiO₂ and ZnO visible light active. *ChemInform* **170**, 560–569 (2010)
34. M. Samadi, M. Zirak, A. Naseri, E. Khorashadizade, A.Z. Moshfegh, Recent progress on doped ZnO nanostructures for visible-light photocatalysis. *Thin Solid Films* **605**, 2–19 (2016)
35. R. Saravanan, S. Karthikeyan, V.K. Gupta, G. Sekaran, V. Narayanan, A. Stephen, Enhanced photocatalytic activity of ZnO/CuO nanocomposite for the degradation of textile dye on visible light illumination. *Mater. Sci. Eng., C* **33**, 91–98 (2013)
36. J.X. Sun, Y.P. Yuan, L.G. Qiu, X. Jiang, A.J. Xie, Y.H. Shen, J.F. Zhu, Fabrication of composite photocatalyst g-C₃N₄-ZnO and enhancement of photocatalytic activity under visible light. *Dalton Trans.* **41**, 6756–6763 (2012)
37. R. Saravanan, E. Sacari, F. Gracia, M.M. Khan, E. Mosquera, V.K. Gupta, Conducting PANI stimulated ZnO system for visible light photocatalytic degradation of coloured dyes. *J. Mol. Liq.* **221**, 1029–1033 (2016)
38. C.G. Tian, Q. Zhang, A.P. Wu, M.J. Jiang, Z.L. Liang, B.J. Jiang, H.G. Fu, Cost-effective large-scale synthesis of ZnO photocatalyst with excellent performance for dye photodegradation. *Chem. Commun.* **48**, 2858–2860 (2012)
39. X. Zhang, L.Z. Zhang, T.F. Xie, D.J. Wang, Low-temperature synthesis and high visible-light-induced photocatalytic activity of BiOI/TiO₂ heterostructures. *J. Phys. Chem. C* **113**, 7371–7378 (2009)
40. L.P. Xu, Y.L. Hu, C. Pelligra, C.H. Chen, L. Jin, H. Huang, S. Sithambaram, M. Aindow, R. Joesten, S.L. Suib, ZnO with different morphologies synthesized by solvothermal methods for enhanced photocatalytic activity. *Chem. Mater.* **21**, 2875–2885 (2009)

Publisher's Note Springer Nature remains neutral with regard to jurisdictional claims in published maps and institutional affiliations.